Int J Thermophys (2008) 29:2046–2054
DOI 10.1007/s10765-008-0532-8

Thermal-Pulse Tomography of Space-charge and Polarization Distributions in Electret Polymers

Axel Mellinger · Rosaura Flores-Suárez · Rajeev Singh · Michael Wegener · Werner Wirges · Reimund Gerhard · Sidney B. Lang

Published online: 15 November 2008

Abstract A new, non-destructive technique for the analysis of electret materials is presented. Thermal-pulse tomography produces three-dimensional images of space-charge and polarization distributions with a lateral resolution of better than 50 μm and a depth resolution of less than 0.5 μm. A focused-pulsed laser heats a circular spot on the opaque upper electrode. While diffusing through the sample, the thermal pulse causes local changes in the sample geometry or dielectric properties, resulting in a short-circuit current in the presence of space charge or electric dipoles. From the transient current, the distribution of the internal electric field can be reconstructed by means of scale transformation or regularization methods.

Keywords Electret · LIMM · Polarization · Polyvinylidene fluoride · Space charge · Thermal-pulse tomography

A. Mellinger · R. Flores-Suárez · R. Singh · M. Wegener · W. Wirges · R. Gerhard
Institute of Physics and Astronomy, University of Potsdam, 14476 Potsdam-Golm, Germany

A. Mellinger (✉)
Department of Physics, Central Michigan University, Mount Pleasant, MI 48859, USA
e-mail: axel.mellinger@cmich.edu

R. Singh
Department of Electronics and Communication, University of Allahabad, Allahabad 211002, UP, India

Present Address:
M. Wegener
Fraunhofer Institute for Applied Polymer Research, 14476 Potsdam-Golm, Germany

S. B. Lang
Department of Chemical Engineering, Ben-Gurion University of the Negev, P.O.B. 653,
Beer Sheva 84105, Israel

1 Introduction

Electret materials are the key to many sensor and actuator applications, such as pressure-sensitive devices, motion sensors, flat loudspeakers, etc. [1]. Research and development in this field requires a non-destructive technique to measure the distribution of the internal electric field caused by embedded space charges or electric dipoles. Since the 1970s, a number of techniques for probing charge and polarization depth profiles have been developed (see the reviews [2–4] and the references therein). Among these, thermal methods are attractive because they provide sub-μm depth resolution at moderate cost and can often be applied in situ for, e.g., experiments in a vacuum environment. The basic concept is to provide an external stimulus in the form of a thermal step, pulse, or wave which propagates through the dielectric medium, thus causing local changes in the geometry or the dielectric properties of the material under study. These changes in turn give rise to a short-circuit current between the metal electrodes at the front and rear surfaces which contain information on the depth-profile of the internal electric field. Thermal profiling has been implemented both in the frequency domain (commonly referred to as the laser intensity modulation method (LIMM) [5]), and in the time domain (thermal pulse (TP) [6] and thermal step [7] methods). It is related to photopyroelectric measurements with pulsed lasers [8,9].

In most published thermal profiling techniques, the lateral extension of the heated zone was large compared to the sample thickness, thus yielding one-dimensional information only. Nevertheless, several attempts were made or suggested [10–12], where the thermal excitation was confined to a small region on the sample surface. Scanning the thermal excitation spot across the sample then yields three-dimensional images of the polarization or space-charge distribution. As laser beams can be brought to a tight focus by suitable optics, the focused LIMM method has the potential for high lateral resolution. However, its relatively slow data acquisition speed often required a compromise between full depth-resolution with a limited number of in-plane data points [13], or larger, high-resolution area maps at selected modulation frequencies [12,14]. Thermal-pulse measurements, however, can be carried out up to 50 times faster than a comparable LIMM scan, as was recently demonstrated in a direct comparison [15] of LIMM and TP which showed excellent agreement between the two techniques (Fig. 1). This triggered the implementation of thermal-pulse tomography (TPT) [16], as described in the following sections.

2 Experimental Setup

The TPs are generated via the absorption of short light pulses by an opaque metal (Cu or Al) electrode. Typically, pulses with an energy of 10 μJ to 500 μJ [generated with a Q-switched, frequency-doubled Nd:YAG laser (Polaris III, New Wave Research)] are focused to spot sizes between 40 μm and 400 μm in diameter. The pulse duration of 5 ns is much shorter than the inverse preamplifier bandwidth (see below) and hence has no effect on the depth resolution. The samples are positioned in the laser beam with a computer-controlled X–Y translation stage (ERLIC 85, OWIS GmbH) and a manual Z translation stage. Optionally, adding a rotary stage allows the investigation

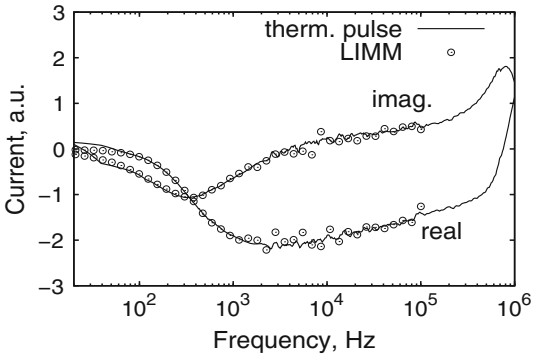

Fig. 1 Comparison of the Fourier-transformed thermal-pulse signal (*solid line*) and the LIMM spectrum (*open circles*) of a volume-charged PTFE film of 17 µm thickness. Data acquisition time was 40 s for the TP signal vs. 30 min for the LIMM curve (*source*: from [15])

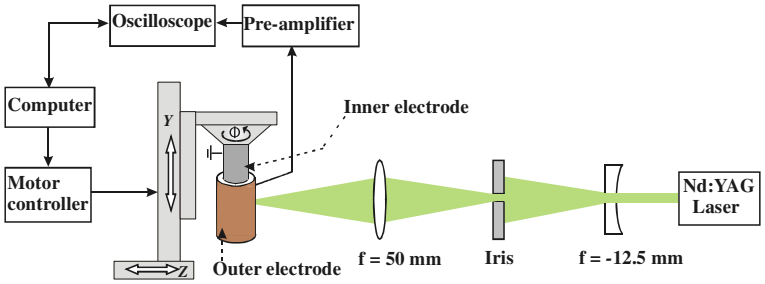

Fig. 2 Experimental setup for focused TPT. The depicted configuration was used for the study of cylindrical geometries (i.e., piezoelectric coaxial cables) (*source*: from [26])

of piezoelectric polymer cables (cf. Fig. 2). The short-circuit current is amplified by a low-noise Stanford Research SR570 current-to-voltage converter and sampled at a typical rate of 10 Msamples/s with a digital storage oscilloscope (Agilent 54833A). Operating in short-circuit mode keeps the RC time constant small, resulting in a high bandwidth, and hence a good depth resolution. With a typical preamplifier bandwidth of 100 kHz, a depth resolution of less than 0.5 µm is achieved. In order to improve the signal-to-noise ratio, up to 50 pulses may be averaged for each beam pointing. As each transient has approximately $N = 512{,}000$ data points, the total amount of raw data for a 2 kpixel pyroelectric image is of the order of 4 GB.

3 Theory and Data Processing

The propagation of the thermal wave in the sample is described by the heat-conduction equation,

$$\nabla^2 T(x, y, z, t) = \frac{1}{D} \frac{\partial T(z, t)}{\partial t}, \tag{1}$$

where $T(x, y, z, t)$ is the temperature and D is the thermal diffusivity of the material. When the size of the heated spot is much larger than the sample thickness d, a one-dimensional solution $T(z, t)$ is usually sufficient [17]. The validity of this assumption

in the present case will be discussed in Sect. 4.1. In the presence of a polarization or space-charge, the TP in a sample with an electrode area A gives rise to the current [2]

$$I_{\sim}(t) = \frac{A}{d} \int_0^d g(z) \frac{\partial T_{\sim}(z,t)}{\partial t} \, \mathrm{d}z \tag{2}$$

with the distribution function

$$g(z) = (\alpha_\varepsilon - \alpha_z) \int_0^z \rho(\xi) \, d\xi + p(z), \tag{3}$$

where α_ε is the temperature coefficient of the permittivity, α_x the thermal expansion coefficient, $\rho(z)$ the space-charge density, and $p(z)$ is the pyroelectric coefficient.

The framework of Eqs. 1–3 can be solved for $g(z)$, $\rho(z)$, or $p(z)$, either in the time or in the frequency domain. For a thermal-pulse experiment, the time domain appears to be the obvious choice. However, to preserve the phase information in the signal, it is crucial to remove any phase shift introduced by the amplifier electronics [15], which is most easily done in the frequency domain. Thus, the transient thermal-pulse current $I(t_k)$, $k = 1 \ldots N$, is converted to the frequency domain using the discrete fast Fourier transform [18] and divided by the (complex) preamplifier gain $\tilde{\alpha}$:

$$\tilde{J}(f_n) = \frac{\Delta t}{\tilde{\alpha}(f_n)} \sum_{k=0}^{N-1} I(t_k) \mathrm{e}^{-2\pi i k n/N}, \tag{4}$$

with the discrete frequency points defined by

$$f_n = \frac{n}{N \Delta t}, \qquad n = 1 \ldots \frac{N}{2}, \tag{5}$$

where Δt is the sampling interval.

Solving Eq. 2 (a Fredholm integral equation of the first kind) is known to be an ill-posed problem. Several techniques have been developed in order to extract physically meaningful solutions $g(z)$ from the experimental data, such as Tikhonov regularization [19] (sometimes combined with polynomial approximations [20,21]), a scale-transformation method [22], iterative approaches [23], and *Monte Carlo* techniques [24]. In the present study, regularization in combination with the L-curve method [25] was used for thinner samples ($d < 25\,\mu\mathrm{m}$) [16], whereas the simpler scale-transformation approach was used when the near-surface polarization in thicker samples was of interest [26]. A general solution for the three-dimensional equivalent of Eq. 2 is currently under development. By taking into account lateral thermal diffusion, an effective increase in lateral resolution is expected.

4 Results and Discussion

4.1 Polyvinylidene Fluoride Films

Initial tests of the new tomographic technique were carried out on films of polyvinylidene fluoride (PVDF), which had received a structured polarization by applying an electric field of approximately $100\,\mathrm{MV}\cdot\mathrm{m}^{-1}$ to a patterned, 'T'-shaped electrode (Fig. 3a), which was later overcoated with a light-absorbing 200 nm Cu electrode (Fig. 3b). From the thermal-pulse data, the polarization map was calculated by means of Tikhonov regularization, with the regularization parameter being obtained via the L-curve method [25]. The lateral resolution of 200 µm (limited here by the chosen laser spot size) is clearly superior compared to recent acoustic approaches [27].

Detailed studies of the lateral resolution were carried out by performing a series of one-dimensional scans across the edge of the 'T' electrode (parallel to the Y-axis in Fig. 3c). The width of the poled/unpoled transition region in the PVDF sample is determined by electrical stray fields, and is expected to be less or equal to the sample thickness of 11 µm. For a laser beam waist of 40 µm, one would therefore expect a lateral resolution equal to this spot size. However, Fig. 4a shows a strong dependence of the lateral resolution on depth, caused by the very different thermal diffusivities $D = \kappa/(c\rho)$ of the metal electrode and the polymer material (where κ denotes the thermal conductivity and $c\rho$ the heat capacity per unit volume). As the diffusion length at a given time t is $\ell = \sqrt{Dt}$, the lateral diffusion speed of the TP in the electrode (with a diffusivity of approximately $10^{-4}\,\mathrm{m}^2\cdot\mathrm{s}^{-1}$) is some 30× faster than the vertical diffusion speed into the polymer (where $D \approx 10^{-7}\,\mathrm{m}^2\cdot\mathrm{s}^{-1}$). As a consequence, the

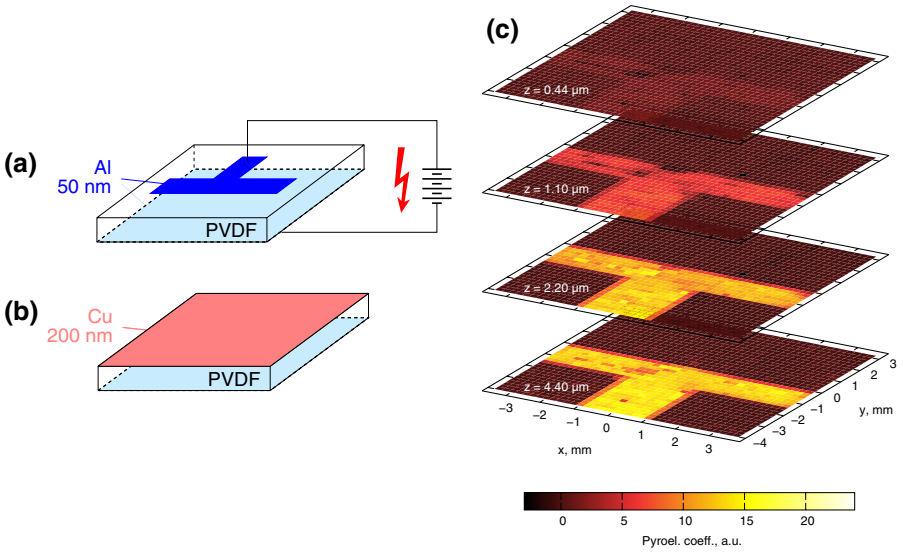

Fig. 3 Preparation of PVDF test samples with (**a**) a patterned Al electrode used for poling, (**b**) the final Cu electrode used for the TP experiments, and (**c**) polarization map at different depths

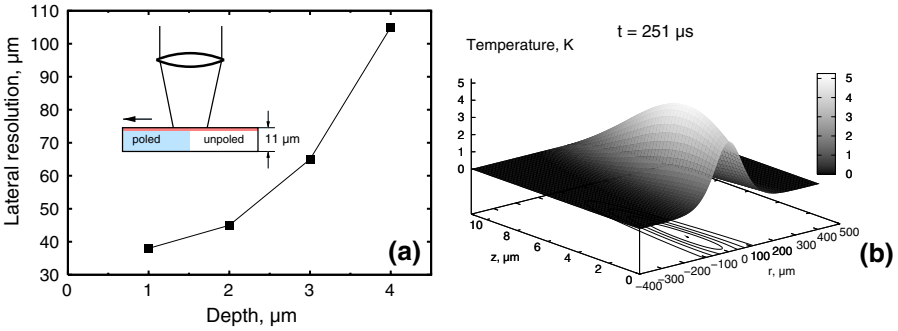

Fig. 4 (**a**) Depth-dependence of the lateral resolution in PVDF at a beam spot size of approximately 40 µm. The data were obtained by scanning the poled/unpoled transition region, as shown in the inset. (**b**) Temperature distribution in the electrode and polymer 251 µs after the laser pulse, calculated by means of the finite-element method [28]. Note the different diffusion lengths in the radial (r) and depth (z) directions

heated front electrode cools more rapidly than the polymer, thus turning from a heat source in to a heat sink, so that the point of maximum temperature starts moving into the polymer (Fig. 4b). Recent finite-element calculations of the temporal and spatial evolution of the heat pulse confirmed this qualitative discussion [28]. Enhancing the lateral resolution thus depends on the ability to find a surface electrode with good electrical conductivity to maintain the short-circuit condition, but low thermal diffusivity. In addition, a solution of the LIMM Eq. 2 taking into account the three-dimensional heat diffusion needs to be found. In regions with a strong in-plane variation of the polarization, a 3-D analysis could enhance the lateral resolution.

Besides providing a test case for the lateral spatial resolution, PVDF films showed unexpected inhomogeneities in the polarization when subjected to bipolar electric fields. In order to investigate the polarization switching behavior, the poling cycle was interrupted at various levels of the electric field. Figure 5 shows an incomplete switching in the bulk, and a polarization pinning at depths up to 1 µm. Polarization pinning

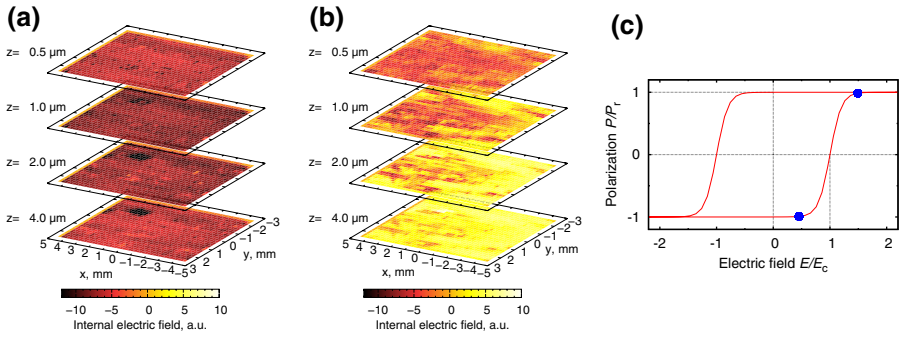

Fig. 5 Polarization maps in PVDF poled at fields of (**a**) $25\,\mathrm{MV\cdot m^{-1}}$ and (**b**) $82\,\mathrm{MV\cdot m^{-1}}$. The poling fields were applied by cycling the electric field through one or more full hysteresis loops (**c**) and stopping at the respective field, indicated by *solid circles* on the hysteresis curve. P_r and E_c denote the remanent polarization and the coercive field, respectively

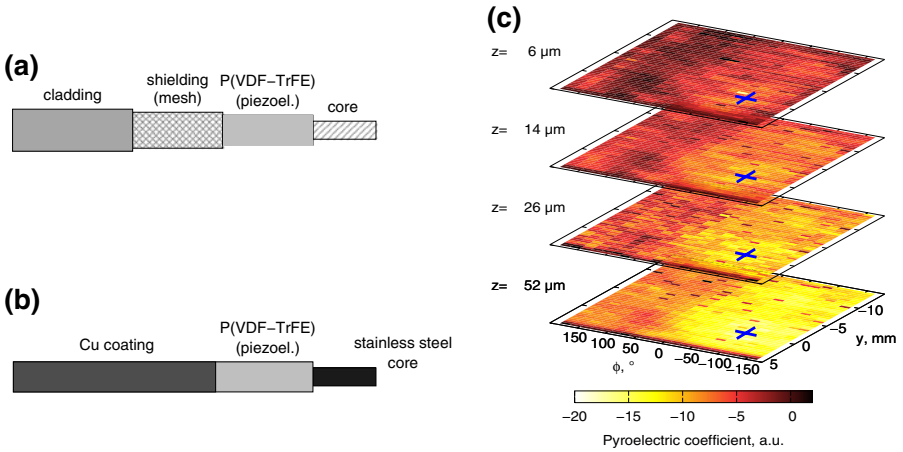

Fig. 6 Schematic view of a piezoelectric sensor cable: (**a**) as received, (**b**) after preparation for TPT. The stainless steel pin serves both as inner electrode and as mounting point. (**c**) Polarization map of a sensor cable poled with a single stationary needle at −25 kV (right). The *crosses* mark the needle position (*source*: from [26])

has been observed in PVDF by other authors, but has been attributed to material fatigue after more than 10^4 poling cycles [29]. Further studies are needed to determine the cause of the incomplete switching.

4.2 PVDF–TrFE Coaxial Sensor Cables

Coaxial sensor cables with an active layer made of piezoelectric PVDF–TrFE copolymer (cf. Fig. 6a) have found important applications in traffic monitoring and intrusion detection. Typically, they are poled (and thus given their piezoelectric properties) by subjecting the extruded cables to a corona discharge formed by a series of high-voltage points around the cable [30]. Recently, polarization maps were obtained with the new tomographic technique from cables poled either in the above-described continuous process or in the laboratory with a single stationary needle [26]. The cables were prepared for TPT measurements by replacing their soft wire core with a stainless steel pin, removing their protective cladding and shielding, and coating the active PVDF–TrFE layer with a Cu electrode (Fig. 6b). Samples poled in the continuous process show a rather uneven distribution that can be attributed to the fact that any point on the cable was exposed to the corona discharge for no more than 300 ms at the given drawing speed. The laboratory-poled cables, on the other hand, show a smooth polarization centered on the needle position in a region approximately 50–100° wide (cf. Fig. 6c), depending on the poling voltage [26]. It was thus shown that optimum poling can be achieved with a set of four to six corona needles at slow drawing speeds.

4.3 Space-charge Electrets

TPT is also suitable for mapping the charge distribution in space-charge electrets. For example, films of polytetrafluoroethylene (PTFE, thickness 17 µm) were irradiated

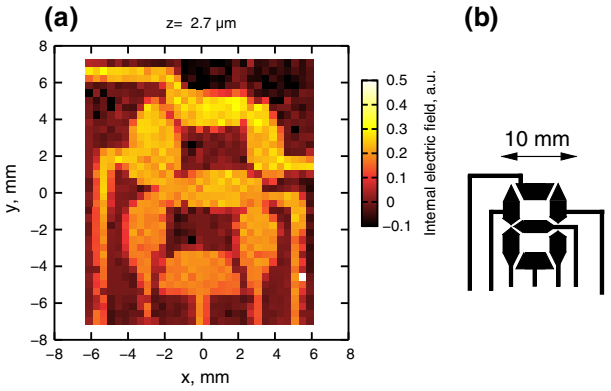

Fig. 7 Internal electric field in electron-beam irradiated PTFE film: (**a**) field distribution at a depth of $z = 2.7$ µm and (**b**) shadow mask used for charging (*source*: from [28])

with a monoenergetic electron beam (15 keV) through a shadow mask (cf. Fig. 7b). The resulting patterned space-charge distribution is shown in Fig. 7a. All the details of the mask are very well reproduced by the space-charge pattern. For the maximum signal-to-noise ratio, the samples had to be glued to a substrate in order to avoid thermo-elastic resonances [31].

5 Conclusions

TPT is a versatile, non-destructive method for obtaining tomographic images of space-charge and polarization distributions in electret materials. A depth-dependent lateral resolution of 38 µm to 105 µm has been achieved in ferroelectric PVDF films. Non-planar geometries can be studied as well, as was demonstrated on piezoelectric PVDF-TrFE sensor cables. Work is in progress to improve the lateral resolution by optimizing the electrode material with respect to thermal conductivity and thermal diffusivity, as well as through a numerical data-analysis procedure taking into account the in-plane thermal diffusion.

Acknowledgments The authors would like to thank Lucas F. Santos (Instituto de Física de São Carlos, Brazil) for providing the electron-beam charged PTFE samples. The equipment was funded in part by the European Regional Development Fund. R.S. acknowledges financial support from the German Academic Exchange Service (DAAD).

References

1. G.M. Sessler, R. Gerhard-Multhaupt (eds.), *Electrets*, 3rd edn., vol. 1–2. (Laplacian Press, Morgan Hill, CA, 1999)
2. S. Bauer, S. Bauer-Gogonea, IEEE Trans. Dielect. Elect. Insul. **10**, 883 (2003)
3. J. Lewiner, S. Holé, T. Ditchi, IEEE Trans. Dielect. Elect. Insul. **12**, 114 (2005)
4. R.J. Fleming, IEEE Trans. Dielect. Elect. Insul. **12**, 967 (2005)
5. S.B. Lang, D.K. Das-Gupta, Ferroelectrics **39**, 1249 (1981)
6. R.E. Collins, J. Appl. Phys. **47**, 4804 (1976)

7. A. Toureille, P. Notingher Jr., N. Vella, S. Malrieu, J. Castellon, S. Agnel, Polym. Int. **46**, 81 (1998)
8. H. Coufal, Thin Solid Films **193**, 905 (1990)
9. H. Coufal, A. Mandelis, Ferroelectrics **118**, 379 (1991)
10. Ş. Yilmaz, S. Bauer, W. Wirges, R. Gerhard-Multhaupt, Appl. Phys. Lett. **63**, 1724 (1993)
11. S. Bauer, J. Appl. Phys. **80**, 5531 (1996)
12. B. Ploss, W. Hassler, H. Hulz, G. Kobernik, Proceedings of the 11th IEEE Symposium on Applications of Ferroelectrics (IEEE Service Center, Piscataway, NJ, 1998), pp. 207–210
13. D. Marty-Dessus, L. Berquez, A. Petre, J.L. Franceschi, J. Phys. D: Appl. Phys. **35**, 3249 (2002)
14. A. Quintel, J. Hulliger, M. Wübbenhorst, J. Phys. Chem. B **102**, 4277 (1998)
15. A. Mellinger, R. Singh, R. Gerhard-Multhaupt, Rev. Sci. Instrum. **76**, 013903 (2005)
16. A. Mellinger, R. Singh, M. Wegener, W. Wirges, R. Gerhard-Multhaupt, S.B. Lang, Appl. Phys. Lett. **86**, 082903 (2005)
17. R. Emmerich, S. Bauer, B. Ploss, Appl. Phys. A **54**, 334 (1992)
18. M. Frigo, S.G. Johnson, Proc. IEEE **93**, 216231 (2005)
19. A.N. Tikhonov, A.V. Goncharskii, V.V. Stepanov, I.V. Kochikov, Sov. Phys. Doklady **32**, 456 (1987)
20. S.B. Lang, IEEE Trans. Dielect. Elect. Insul. **11**, 3 (2004)
21. S.B. Lang, J. Mater. Sci. **41**, 147 (2006)
22. B. Ploss, R. Emmerich, S. Bauer, J. Appl. Phys. **72**, 5363 (1992)
23. A. Mellinger, Meas. Sci. Technol. **15**, 1347 (2004)
24. E. Tuncer, S.B. Lang, Appl. Phys. Lett. **86**, 071107 (2005)
25. P.C. Hansen, D.P. O'Leary, SIAM J. Sci. Comput. **14**, 1487 (1993)
26. R. Flores Suárez, A. Mellinger, M. Wegener, W. Wirges, R. Gerhard-Multhaupt, R. Singh, IEEE Trans. Dielect. Electr. Insul. **13**, 1030 (2006)
27. T. Maeno, IEEE Trans. Dielect. Elect. Insul. **8**, 845 (2001)
28. A. Mellinger, R. Singh, M. Wegener, W. Wirges, R. Flores Suárez, S.B. Lang, L.F. Santos, R. Gerhard-Multhaupt, Proceedings of 12th International Symposium on Electrets (IEEE Service Center, Piscataway, NJ, 2005), pp. 212–215
29. S. Sakai, M. Date, T. Furukawa, Jpn. J. Appl. Phys. **41**, 3822 (2002)
30. M. Wegener, R. Gerhard-Multhaupt, IEEE Trans. Ultrason. Ferroelect. Freq. Control **50**, 921 (2003)
31. P. Bloß, H. Schäfer, Rev. Sci. Instrum. **65**, 1541 (1994)